

Review

# An Old Material for a New World: Prussian Blue and Its Analogues as Catalysts for Modern Needs

Isabella Concina 

Division of Materials Science, Department of Engineering Sciences and Mathematics,  
Luleå University of Technology, 97187 Luleå, Sweden; isabella.concina@ltu.se

**Abstract:** Prussian blue analogues (PBAs) have recently emerged as effective materials in different functional applications, ranging from energy storage to electrochemical water splitting, thence to more “traditional” heterogeneous catalysis. Their versatility is due to their open framework, compositional variety, and fast and efficient internal charge exchange, coupled with a self-healing ability that makes them unique. This review paper presents and discusses the findings of the last decade in the field of the catalytic and photocatalytic application of PBAs in water remediation (via the degradation of organic pollutants and heavy metal removal) and the catalytic oxidation of organics and production of organic intermediates for industrial synthesis. Analysis of the catalytic processes is approached from a critical perspective, highlighting both the achievements of the research community and the limits still affecting this field.

**Keywords:** Prussian blue analogues; adsorption; catalysis; Fenton process; persulfate

## 1. Introduction

Prussian blue (PB) and its analogues are experiencing a time of re-discovery: well known since the 18th century as a blue pigment used in paintings, PB is becoming the center of interest for researchers working in diverse application fields ranging from energy storage (batteries and supercapacitors) [1] to catalytic water splitting for the generation of clean fuels [2,3], catalytic water remediation, and so on. PB and Prussian blue analogues (PBAs) possess unique structural, ionic, and electronic properties, which are nowadays recognized as key tools for functional applications.

From a coordination chemistry standpoint, PB is perhaps the most classical example of a mixed-valence coordination complex and can be considered the archetype of this kind of compound. The empirical formula (not considering crystallization water) is  $\text{Fe}_7(\text{CN})_{18}$  and the basic chemical structure features an  $\text{Fe}^{2+}$  ion octahedrally coordinated to the carbon atom of six cyanide ligands (Figure 1), while at the nitrogen atom,  $\text{Fe}^{3+}$  is bound, meaning that the general formula that shows what we are dealing with is  $\text{Fe}_4[\text{Fe}(\text{CN})_6]_3$ .

The intense blue color, known to all thanks to Van Gogh’s paintings, is due to the intervalent charge transfer of an electron between the  $\text{Fe}^{\text{II}}$  to  $\text{Fe}^{\text{III}}$  atoms present in the basic chemical structure).

From a solid-state perspective, PB has a cubic lattice structure (with a unit cell size of 10.2 Å), and two forms of this iron complex are known: the so-called insoluble PB,  $\text{Fe}_4[\text{Fe}(\text{CN})_6]_3 \cdot x \text{H}_2\text{O}$ , and the so-called soluble PB,  $\text{KFe}[\text{Fe}(\text{CN})_6] \cdot n\text{H}_2\text{O}$ . Figure 2 shows the lattice of PBAs, the general formula of which is  $\text{A}_x\text{M}[\text{M}'(\text{CN})_6]_y\Box_{1-y} \cdot n\text{H}_2\text{O}$ , where M and M’ are transition metal ions coordinated to the nitrogen and carbon atoms of the cyanide ligands, respectively. A is an alkali cation and  $\Box$  stands for the vacancies of the  $\text{M}'(\text{CN})_6$  unit in the lattice.

The key feature making PB and PBAs extremely suitable as catalysts is the  $\text{C}\equiv\text{N}$  bridge, which links transition metals capable of existing in different oxidation states: the cyanide triple bond is indeed an outstanding electron shuttle, capable of moving them back



**Citation:** Concina, I. An Old Material for a New World: Prussian Blue and Its Analogues as Catalysts for Modern Needs. *Inorganics* **2024**, *12*, 124. <https://doi.org/10.3390/inorganics12040124>

Academic Editor: José M. Méndez-Arriaga

Received: 14 March 2024

Revised: 15 April 2024

Accepted: 16 April 2024

Published: 22 April 2024



**Copyright:** © 2024 by the author. Licensee MDPI, Basel, Switzerland. This article is an open access article distributed under the terms and conditions of the Creative Commons Attribution (CC BY) license (<https://creativecommons.org/licenses/by/4.0/>).

and forth between the two metals, separated by about a 5 Å distance. Water molecules can coordinate to M, due to the presence of  $M'(CN)_6$  vacancies, meaning that the coordination sphere of M has the general formula  $M(NC)_x(OH_2)_{6-x}$ . The actual catalytic site is M; water molecules can dissociate and leave space to coordinate other species present in the surrounding environment, having a stronger ligand character (the reader can think of the spectrochemical series). Introducing an alternative metal M to iron in the PB structure is easy from a synthesis perspective, and when M has reversible redox capability, this triggers the catalytic skills of PBAs.

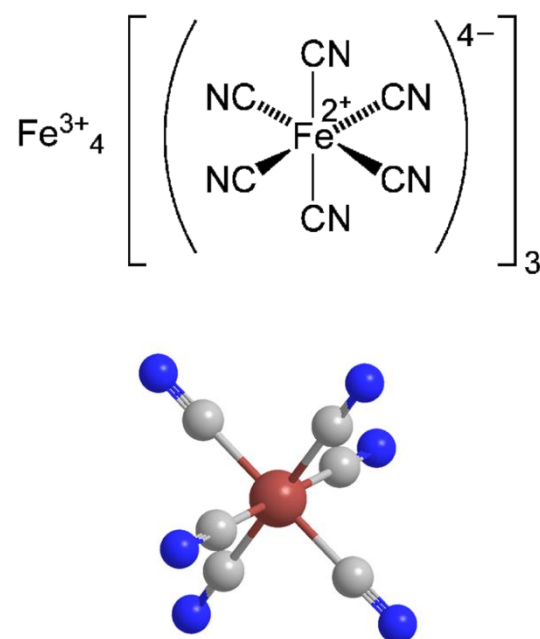


Figure 1. Basic chemical structure of PB. Reprinted from [4].

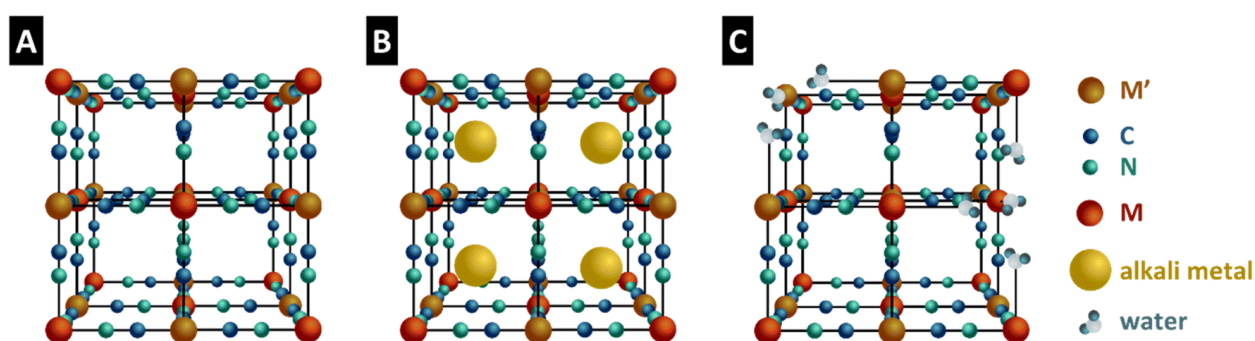


Figure 2. (A) Theoretical PBA lattice. (B) Defect-free “soluble” PBA with alkali ions in the lattice. (C) “Insoluble” PBA lattice with defects, showing water molecules filling the defect sites. Reprinted from Bornamehr et al. [5].

There is, however, another characteristic of these compounds, which is acknowledged as extremely relevant in functional applications and is related to their crystalline structure: PB and PBAs present the capability of inserting species in their crystalline lattice, which makes them excellent materials for use both in energy storage applications and as sorbents to remove unwanted chemicals from water.

PBAs are prepared by several synthetic routes: coprecipitation, hydrothermal synthesis, electrochemical deposition, sonochemical synthesis, and microemulsion. Several reviews have been published that discuss the different outcomes, in terms of structure and composition, obtained by exploiting different synthetic procedures. This discussion is

beyond the scope of the present review and the reader can investigate the topic by referring to references [6–11].

The physical and chemical characteristics of these materials significantly change, depending on the synthetic approach adopted [12], and the preparation method should take into account the desired application. The presence and number of  $M'(CN)_6$  vacancies are, for instance, critical in determining both the crystalline parameters and the number of coordinated water molecules, which eventually affect their performance in all the explored application fields. The bond with water molecules is particularly interesting from a coordination chemistry standpoint, as already mentioned: water binds the transition metal ion linked to the nitrogen of the cyanide ligand. These water molecules can then be easily replaced by stronger ligands that are present in the surrounding environment (the reader can think of the molecular target of a catalytic reaction, bearing functional groups such as carboxylates, amines, ethers, and so on), triggering the electron crosstalk that is strategic for a catalytic cycle.

Another compositional key feature is the nature of the second transition metal: its electronegativity, its capacity to tolerate different oxidation states, and its coordination skills can all play a role in spurring/inhibiting redox processes useful to catalytic processes.

Furthermore, PB and its analogues have a three-dimensional open framework, with interstitial sites that are large enough to accommodate ions with an appropriate radius, which makes them suitable as sorbents.

The first report on the catalytic skills of PBAs dates back to 1984 [13]; Itaya and collaborators reported the reduction of molecular oxygen to water, promoted by Prussian white (the reduced form of PB). Since then, the scientific literature has investigated several other catalytic processes for which PB and its analogues are used as catalysts (or photocatalysts).

This review focuses on the use of PB and its analogues as catalysts and photocatalysts in specific applications, namely: (i) the removal of heavy metals from water (with special reference to cesium); (ii) water remediation; (iii) the synthesis of useful chemicals. We will present the most significant results reported in the last decade. We will not discuss their use in water splitting, for information on which the reader is referred to recent specialized reviews [10,14].

The reader should also be aware that experimental evidence is complemented by calculations more and more often, where computational analysis is carried out in parallel with experiments to support it with a better theoretical understanding of the relevant processes and mechanisms. Furthermore, calculations also quantify (or semi-quantify) the energies involved in chemical reactions (in terms of both synthesis and functional processes), thus providing an important insight into what parameters experimentalists should or should not modulate to improve their materials. The present review is especially intended to support experimentalists with an overview of the recent findings regarding the preparation and application of materials, but [15–19] also provide good examples showing the value of coupling computations with experiments.

## 2. Prussian Blue and Its Analogues as Pollutant Sorbents in Water

The removal of heavy metals from water, although not strictly classifiable as a catalytic process, is an important field of use of PBAs in the field of water remediation. Adsorption of the molecular target is a relevant step in a catalytic reaction, and the knowledge gained from investigations of this process can be strategic in the design of PBA-based catalysts with improved performance.

The removal occurs via the adsorption of metal ions in the porous structure, which is made possible by the coordination ability of PBAs. We will shortly present the results reported in the context of removing heavy metal ions from water, in the hope of providing the reader with some useful insights about the mechanism behind the process, which may be useful for further understanding the catalytic abilities of PBAs.

The most widely investigated metal ion is possibly  $^{137}\text{Cs}^+$ . This radioisotope, with a half-life of longer than 30 years, emits  $\beta/\gamma$  rays (0.514 MeV and 0.662 MeV) [20–22]; it

possesses considerable solubility in water, which makes it a relevant target for removal from the environment. Nuclear wastewater is primarily affected by this contamination, but  $^{137}\text{Cs}^+$  is still present in the environment after nuclear accidents have occurred over time [23]. Most investigations deal with the non-radioactive  $\text{Cs}^+$  for obvious reasons, but a few papers have also studied actual radioisotope removal.

Ishizaki et al. have elucidated the mechanism of adsorption of  $\text{Cs}^+$  by PB in 2013 [24], showing that the hydrated  $\text{Cs}^+$  ions are trapped via lattice defect sites with hydrophilicity, highlighting once more how the crystal structure and the composition of this class of materials deeply affect their performance. Specifically, a high number of water coordination molecules (corresponding to a high quantity of  $[\text{Fe}^{\text{II}}(\text{CN})_6]^{4-}$  vacancies) is associated with the adsorption of hydrated  $\text{Cs}^+$  ions and is accompanied by the elimination of protons from water molecules.

Superparamagnetic nano-sorbents based on PB-coated  $\text{Fe}_3\text{O}_4$  nanoparticles, developed by Thammawong and coworkers [25], were used in sorption experiments to remove different Cs amounts from water (from 50 to 2780 ppm). The adsorption equilibrium was reached in 24 h and the sorbent material could be easily removed by magnetic decantation, which appears to be a convenient strategy that is potentially applicable in real-life scenarios. The adsorption process can be modeled by the Langmuir model (Equation (1)):

$$Q_e = \frac{Q_{\max}kC_e}{1 + kQ_e} \quad (1)$$

where  $Q_e$  evaluates the amount of Cs adsorbed at the equilibrium,  $Q_{\max}$  is the maximum adsorption capacity of the material,  $C_e$  is the equilibrium concentration of the ionic target, and  $k$  measures the affinity constant of the sorbet towards Cs.  $Q_{\max}$  was calculated to be as high as 96 mg/g, with an affinity constant  $k$  of  $4.3 \times 10^{-3}$  L/mg, values that are over the previously reported performance by the soluble form of PB (assessed at as high as 78 mg/g) [26], probably due to the nanometer sizes of the prepared sorbent. The presence of competitive ions ( $\text{Na}^+$ ,  $\text{K}^+$ ,  $\text{Ca}^{2+}$ ,  $\text{Mg}^{2+}$ ), however, significantly lowered the distribution coefficient (a more suitable parameter than  $Q_{\max}$  to evaluate the sorption capability at low  $\text{Cs}^+$  concentrations) from 268 mL/g (no competitor) to 14.3 mL/g (in the presence of  $\text{K}^+$ ), with an order following that of the hydration radii of the cations.

In-situ-generated PB on pure and acid-modified cellulose fiber was tested for cesium (0.2 to 100 ppm) removal from water in a sealed tube maintained under stirring for 24 h at 303 K [27]. The structural analysis showed thin entangled fibers (diameter 10–20  $\mu\text{m}$ ) featuring many internal spaces, with an amount of PB from 26% to almost 41% in weight for the pure and modified cellulose, respectively. Adsorption equilibrium was observed within 6 h, and second-order kinetics was evaluated as the best-fitting model. The authors found maximum cesium adsorption as high as 7.95 and 12.4 mg/g for the unmodified cellulose and the acid-functionalized material, respectively; the difference recorded was exactly the difference in PB loading, thus leading to the conclusion that increasing the PB content was the key factor in increased  $\text{Cs}^+$  removal.

Jung and collaborators synthesized PB in situ on porous polyacrylamide (PAAm) spheres via wet chemistry (Figure 3) [28]. The hybrid system was found to upload an impressive number of  $\text{Cs}^+$  ions (374 mg/g), with fast kinetics (90% of maximum cesium adsorption was reached in 30 min) and superior selectivity against competitive ions ( $\text{Na}^+$ ,  $\text{K}^+$ ,  $\text{Mg}^{2+}$ ,  $\text{Ca}^{2+}$ ), even at a very low concentration of  $\text{Cs}^+$  (10 ppt). This impressive performance was attributed to the microporous structure of the PAAm spheres, coupled with the thin film of PB generated on their surface and covalently bound to it.

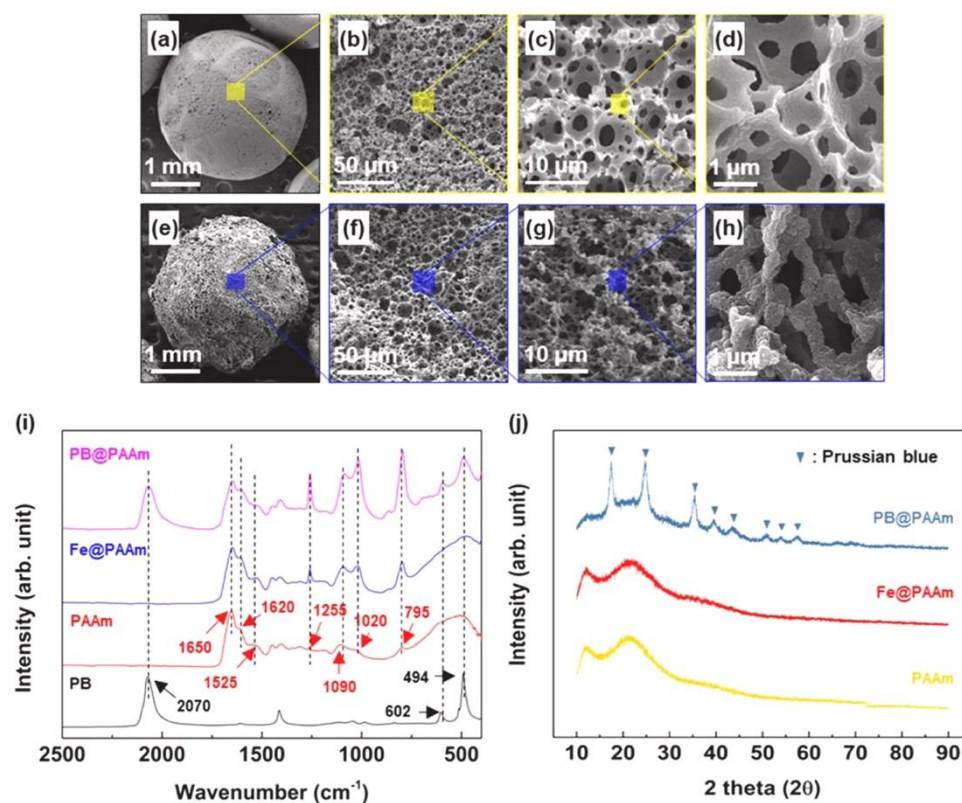


**Figure 3.** SEM images of the PAAm (a–d) before and (e–h) after the fixation of PB nanocrystals. (i) FTIR spectra and (j) XRD patterns for PAAm, over the course of the PB coating process. Reprinted from Ref. [28], with permission from Elsevier.

PB was grown in situ on a lightweight porous ceramic foam by Liu et al. [29]. The foam was based on natural clinoptilolite and could float on water (thus making its recovery after use easy and straightforward). PB was grown on its surface by immersion in  $K_4[Fe(CN)_6]$  in an acidic solution, resulting in the formation of PB wherein some potassium ions were substituted by aluminum. The authors measured a 90% absorption of 100 ppm  $Cs^+$  solution in 5 min (2 g of sorbent was used in the experiment). The claimed mechanism was an ion exchange of  $K^+$ - $Cs^+$  on the surface of the hybrid sorbent, but it is not clear why the material showed a preference towards the latter cation.

Elsewhere, a copper-based PBA was loaded onto a polyvinyl chloride composite membrane through the solvent evaporation method [30]. Proof of the successful synthesis of Co-PBA was provided by XRD and FTIR. The functional material was then tested (1 g/L) as a sorbent for  $Cs^+$  (50 mg/L) in water, upon stirring for 120 min. Pure PBA was also tested for comparison purposes. It was found that this latter substance could remove a higher amount of cesium than when the same material was loaded on the membrane (98.7% vs. 82.3%, respectively), but that the recovery (and subsequent recycling) was harder. Furthermore, the authors found a significant amount of iron in the reaction mixture, highlighting the dissolution of PBA, while the same effect was observed in much smaller amounts for the membrane, which imparted stability to the active material.

PBAs were also investigated as  $Cs^+$  sorbents in hybrid composites with  $TiO_2$  to provide the iron complex with an active substrate that should, on one hand, make its recovery and recycling easier, and, if irradiated with proper light, enhance useful redox processes at the surface of the hybrid sorbent.

PB was photo-deposited on commercial  $TiO_2$  P25 by Kim and coworkers [31] and tested as a sorbent for  $Cs^+$  and  $^{137}Cs^+$ , under dark and UV irradiation conditions. PB generated on  $SiO_2$  was used as a control sample. The outcomes (reported in Figure 4 as the adsorption of cesium ions vs. time for different sorbent systems) showed that: (i) bare

TiO<sub>2</sub> does not contribute at all to Cs<sup>+</sup> removal; (ii) there is an obvious enhancement in Cs<sup>+</sup> adsorption upon UV irradiation that is not detectable when VIS light is used; (iii) the hybrid composite PB-SiO<sub>2</sub>, although showing fair performance as a sorbent under dark conditions, is not affected by light exposure. This interesting investigation, claimed as the first of its kind, shows that the photogeneration of exciton pairs within TiO<sub>2</sub> is responsible for the electrochemical processes undergone by PB (probably a spurred reduction of Fe(III) to Fe(II) and the subsequent formation of Prussian white), which enhances the capability of PB to insert Cs<sup>+</sup> ions in its crystalline lattice (Prussian white is reported to contain two alkali metals instead of one, as with PB). The authors could also demonstrate the adsorption of <sup>137</sup>Cs<sup>+</sup>.

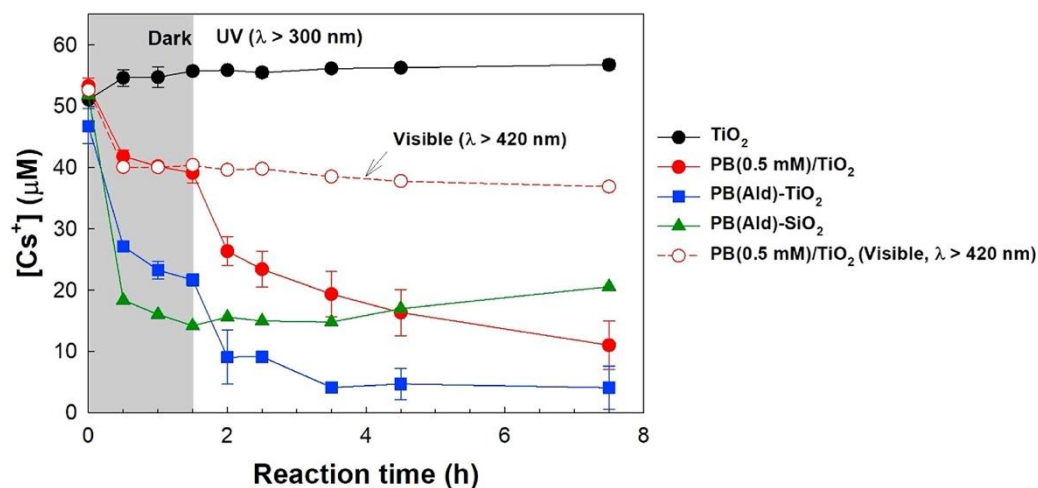


**Figure 4.** Dark adsorption and the photocatalytically enhanced adsorption of Cs<sup>+</sup> ions on TiO<sub>2</sub>, PB/TiO<sub>2</sub>, PB-TiO<sub>2</sub>, and PB-SiO<sub>2</sub>. [Cs<sup>+</sup>]<sub>0</sub> = 50 μM, [TiO<sub>2</sub>] = [PB/TiO<sub>2</sub>] = [PB/SiO<sub>2</sub>] = 5 g/L. Reprinted from Ref. [31], with permission from Elsevier.

PB and its analogues have been coupled with other materials for adsorption purposes, with interesting results.

Chen prepared a PBA on Zn-Ti layered double hydroxides (LDH) that were then granulated by calcium alginate [32], which showed an adsorption capacity of as high as 254.2 mg/g in 60 min, with kinetics following the Langmuir model. The proposed adsorption mechanism, as confirmed by the analysis of metal content in the reaction mixtures, was suggested to be, once more, the displacement of potassium ions from the PBA lattice.

Reduced graphene oxide (RGO) was also used by several researchers as an active substrate/scaffold for PBAs in sorbent applications.

Huo et al. prepared Ni-PBA in the form of nanoparticles (40–50 nm) on RGO [33]. The synthesis was performed by anchoring the Ni<sup>2+</sup> ions on RGO, thanks to its carboxylic groups, followed by impregnation on a solution containing Fe(CN)<sub>6</sub><sup>3-</sup>. Adsorption tests were carried out for 72 h and showed three steps: first, a rapid decrease in the Cs<sup>+</sup> concentration in the first 5 h, followed by a slack stage (up to 24 h) leading to equilibrium (24–72 h). The 3D RGO was thought to provide more accessible sites for cesium ions, coupled with a hydrophilic surface facilitating the mass transfer of cesium, reaching an adsorption capacity of 204.9 mg/g. The analyses suggested that this adsorption consists of different processes, including ion exchange (Cs<sup>+</sup> replacing K<sup>+</sup>), ion trapping (Cs<sup>+</sup> being trapped by the crystalline PBA structure), and complexation interaction. This latter process would not involve the Ni-PBA, however, but instead involves the oxygen-rich RGO edges, which could bind the Cs<sup>+</sup> ions.

A similar approach was used by Li et al. [34], who prepared an RGO aerogel with a ternary PBA based on Ni, which uploaded up to 226.98 mg/g of Cs<sup>+</sup>.

RGO was revealed as a good support for PBA nanoparticles, which could be observed gathered in groups on the RGO surface (Figure 5). It should, however, be noted that RGO was not simply a spectator in the process but also contributed to the removal of cesium ions. In this case, too, several processes were considered to be involved in adsorption (ion exchange and ion trapping).

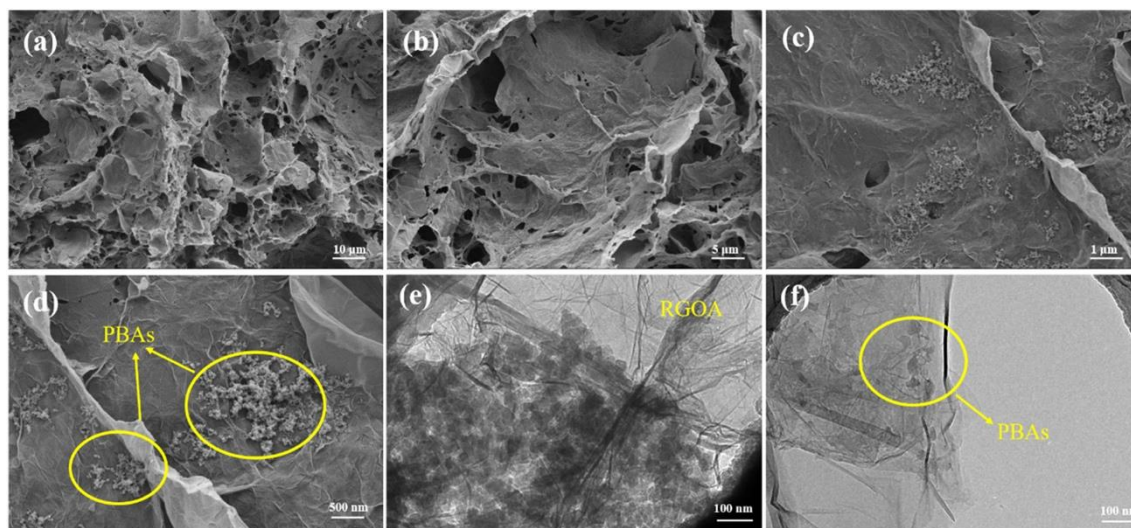


**Figure 5.** SEM images (a–d) and TEM images (e,f) of RGO doped with Ni-PBA. Reprinted from Ref. [34], with permission from Elsevier.

Apart from cesium, other metal ions have proven to be possible to remove with PBAs. Ferreira-Neto and collaborators used PB as a co-catalyst to support  $\text{TiO}_2$  action in the reduction of Cr(VI) to Cr(III) [35].  $\text{TiO}_2$  or  $\text{SiO}_2\text{-TiO}_2$  nanoparticles and aerogels were used as the main catalysts and their surface was modified with nanocrystalline PB by photodeposition. This interesting paper was based on the idea that PB can mediate the necessary charge exchange between the semiconductor and the heavy metal ions. Different composites were prepared and their performance was evaluated: 10 ppm of  $\text{K}_2\text{Cr}_2\text{O}_7$  in water was tested in a 70 mL solution containing 35 mg of catalyst, left under stirring in the dark for 30 min, and then irradiated with UV light without any pH adjustment. Less than 10% of the initial Cr(VI) amount was adsorbed under dark conditions, suggesting the occurrence of a real catalytic process induced by light irradiation. The bare semiconductor nanoparticles showed a fairly good capability of reducing Cr(VI), but all were overtaken by the PB-deposited composites, with results ranging from about 80% to 100% Cr(VI) removal, depending on the specific catalyst. The mechanism attributed to this effect was the transfer of photogenerated electrons from the conduction band of titanium to PB, which was then reduced to Prussian white. The reduced sites were the actual catalytic species, thanks to possessing a longer lifetime than that of electrons in titanium.

A polyaniline nanocomposite modified with Co-Fe PBA was tested for the removal of rubidium ions by Moazezi [36]. PBA polyhedral particles with sizes ranging from 80 to 100 nm were observed on PANI; the system has a surface area of  $35.21 \text{ m}^2/\text{g}$ , with an average pore diameter of  $2.175 \text{ \AA}$ . Rubidium removal was investigated by using a 100 ppm  $\text{Rb}^+$  water solution, which was left in contact with different sorbent amounts (1 to 5 g/L) for 500 min. In the best conditions, the authors observed the almost complete removal of rubidium ions (>98%) in 500 min, calculating pseudo-second-order kinetics for the adsorption process.

Other heavy metals where the removal by PBAs is discussed in the literature are thallium [37] (with impressive results of 528 mg/g adsorbed on magnetic PB nanoparticles, as published by Zhang and collaborators) [38], copper, cobalt, nickel and lead (magnetic PB) [39], and rubidium [36].  $\text{Pb}^{2+}$  was effectively removed by using magnetic  $\text{Mn}_3[\text{Co}(\text{CN})_6]_2 \cdot n \text{ H}_2\text{O}$  PBA [40], a Mn-PBA in which the surface and active sites were

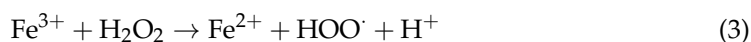
engineered [41]. Magnetic PB-based composites were also used as sorbents for Cd<sup>2+</sup> removal [42,43].

To conclude this section, it seems worth also mentioning the application of PBA-based electrodes (Cu, Mn, and Zn) for water desalination (the removal of Na<sup>+</sup> and Ca<sup>2+</sup>) through intercalation [44].

### 3. Catalytic Degradation of Organic Pollutants

Many investigations about the catalytic skills of PB and PBAs are based on their capacity to activate hydrogen peroxide (through the Fenton reaction) or persulfate. The reader is referred to a recent review by Dong et al. for more on this topic [11].

Fenton catalysis [45] involves the generation of hydroxyl radical species (•OH) from hydrogen peroxide through reduction with set amounts of a certain metal ion, most commonly Fe(II). These radicals are then the actual species attacking the organic pollutants (thanks to their very positive redox potential of 2.84 V vs. NHE). In the Fenton reaction, Fe(II) is oxidized by hydrogen peroxide to Fe(III), with the subsequent formation of a hydroxyl radical and a hydroxide ion (Equation (2)). Another molecule of H<sub>2</sub>O<sub>2</sub> then reduces Fe(III) back to Fe(II), with the formation of the hydroperoxyl radical and a proton (Equation (3)), so that the net reaction (Equation (4)) is the disproportionation of hydrogen peroxide generating different oxygen radicals, with water as the byproduct.



Another relevant process for which PBAs are used is the activation of persulfate; this chemical possesses a strong oxidizing capability due to its redox potential of 2.01 V, and it can generate reactive species (especially the sulfate radical and hydroxyl radical) through several activation paths [46].

The Fenton process and persulfate activation are classified as among the advanced oxidation processes (AOPs), which are currently considered the most interesting chemical reactions for water remediation.

#### 3.1. Removal of Dyes

Nossol et al. investigated the degradation of methyl orange (MO) when photo- and electro-photo-catalyzed by PB generated on CNTs on an ITO glass substrate [47]. The studies were conducted in  $2.5 \times 10^{-7}$  M of MO in a 0.1 M KCl solution containing 1 mM of H<sub>2</sub>O<sub>2</sub>. Photocatalytic degradation achieved 37% MO degradation in 160 min, while in the corresponding photoelectrochemical process, 96% MO was reduced within the same reaction time (the performances of bare CNTs and bare PB were lower). The authors applied a potential of 0.0 V to Ag/AgCl, at which PB is reduced to Prussian white, allowing for the regeneration of the ferrous ion, which is efficient at cycling the reaction. Further tests showed that the CNTs imparted stability to PB, which detached from the ITO glass support when deposited alone. Furthermore, an increase in the number of electroactive sites and in the rate of heterogeneous electron transfer supported by the CNTs was also claimed. The CNTs, then, acted as a booster of PB functional skills.

A hierarchical porous RGO/PB polypyrrole (PPy) aerogel was tested for the degradation of Rhodamine B (RhB) by Tong and coworkers in a photo-Fenton reaction [48]. Different reaction conditions were tested, and the optimal setup involved 10 mg of catalyst for a 10 ppm RhB solution at a pH adjusted to 6.18, with 100 μL H<sub>2</sub>O<sub>2</sub> in addition. Under these conditions, 95.2% of RhB was degraded in 30 min. The generated PPy could adhere neighboring GO sheets, thereby inducing a 3D material. Meanwhile, the reducibility of pyrrole monomers reduced the groups on the GO surface and the excess of Fe<sup>3+</sup> could react with K<sub>4</sub>[Fe(CN)<sub>6</sub>] producing PB.

The aerogel was obtained by a simple, albeit effective, procedure:  $\text{Fe}^{3+}$  ions were adsorbed onto the GO sheets through electrostatic attraction, then the polymerization of pyrrole was initiated through oxidation directly onto the GO surface.

A 3D network with interconnected macropores was observed, with PPy being present on the nanosheet surface (red arrows in Figure 6). The mesopores were believed to provide channels for the photo-Fenton process, speeding up the diffusion of the organic target. It should be noted that a system of PB + RGO/PPy was also tested, showing a slower but comparable performance with the hybrid catalyst. This latter was also active in the absence of light, which, however, spurred on the reaction. Hydroxyl radicals were found to be the main active species in the process through trapping experiments. The thermodynamic parameters of the reaction,  $\Delta H$ ,  $\Delta S$ , and  $\Delta G$ , were calculated to be as high as 35 kJ/mol, 96.5 J/mol, and 6.4 kJ/mol, respectively at 298 K, indicating the endothermic, chaotic, and non-spontaneous nature of RhB degradation.

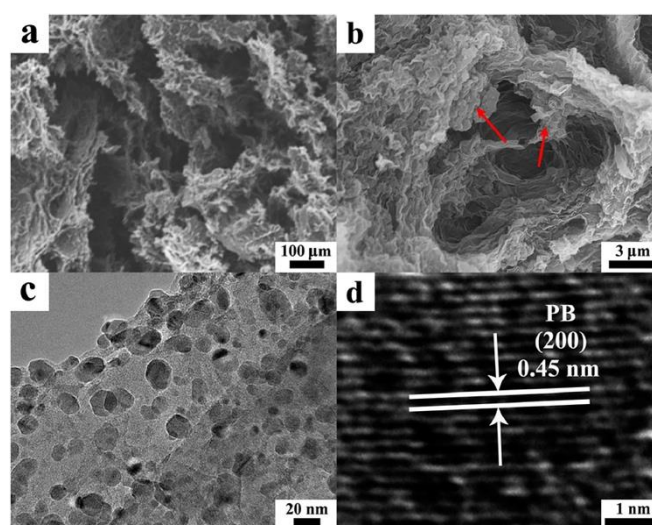


**Figure 6.** (a,b) SEM images of rGO/PB/PPy aerogel at different magnifications; (c) TEM image of rGO/PB/PPy aerogel; (d) HRTEM image of PB NPs. Reprinted from Ref. [48], with permission from Elsevier.

Li and collaborators used a PB/TiO<sub>2</sub> nanocomposite in a photo-Fenton process against RhB (and other organics, such as salicylic acid, m-cresol, and iso-phorone) [49]. PB was deposited in situ on TiO<sub>2</sub> P25 powder at different molar ratios of PB:TiO<sub>2</sub>. The catalyst amount used in the degradation tests was as high as 50 mg in a 50 mL RhB solution (with 12 mg/L as the initial concentration), allowing the mixture to reach adsorption-desorption equilibrium in 30 min (no considerable adsorption of RhB on the PB/TiO<sub>2</sub> catalyst was observed). Either UV or VIS light was used, and different amounts of hydrogen peroxide were employed. The synthesis resulted in the formation of well-crystallized PB nanoparticles on the TiO<sub>2</sub> P25 surface, without the formation of any thin film. Also in this case, the idea behind the fabrication of such a composite was that PB could act as a mediator in the generation of ROS via H<sub>2</sub>O<sub>2</sub> activation by exploiting the photogenerated charges within the semiconductor. Mössbauer spectroscopy was used to investigate the oxidation and spin states of iron in the PB. An increase in low-spin Fe(III) was observed during the RhB degradation reaction when H<sub>2</sub>O<sub>2</sub> was added to the mixture, even though, after UV irradiation, its percentage went back to its original value. Based on this finding, the authors then proposed that TiO<sub>2</sub> photoelectrons could reduce low-spin Fe(II), thus giving the fabrication of composites full justification. The removal of RhB (analyzed by UV-VIS spectroscopy and TOC) was found to be different according to the adopted reaction conditions, reaching a removal efficiency of as high as 95.6% and a TOC removal efficiency of 38.5% in 30 min in the best case. It is important to add two remarks to our discussion of this investigation: (i) an excess of PB on the TiO<sub>2</sub> surface hindered UV absorption by the

semiconductor, thus lowering the catalytic performance; (ii) the hybrid system was also active under VIS irradiation (thanks to PB).

An interesting investigation on dye degradation catalyzed by PB was proposed by Liu et al. [50]. Although older than 10 years, this study is worth citing here, since it tries to shine a light on a phenomenon that is seldom investigated: the effect of metal cations in a reaction mixture that is subjected to a photo-Fenton process. PB nanoparticles (diameter 30–50 nm) were synthesized by the usual coprecipitation approach. RhB, Malachite Green (MG), and Methyl Orange (MO) degradation was tested under VIS light irradiation ( $\lambda > 420$  nm) in the presence of potassium salts and the corresponding sodium salts. The authors remarked upon two effects: (1) the RhB degradation was greater when potassium salts were added to the solution, compared with sodium salts with the same anion; (2) the reaction rate was also higher. A dramatic difference, for instance, was observed in the presence of either KCl (100% MG degradation) or NaCl (29% degradation). The effect of KCl concentration was also investigated (see Figure 7, left panel), showing that the higher the salt concentration was, the better the dye degradation.

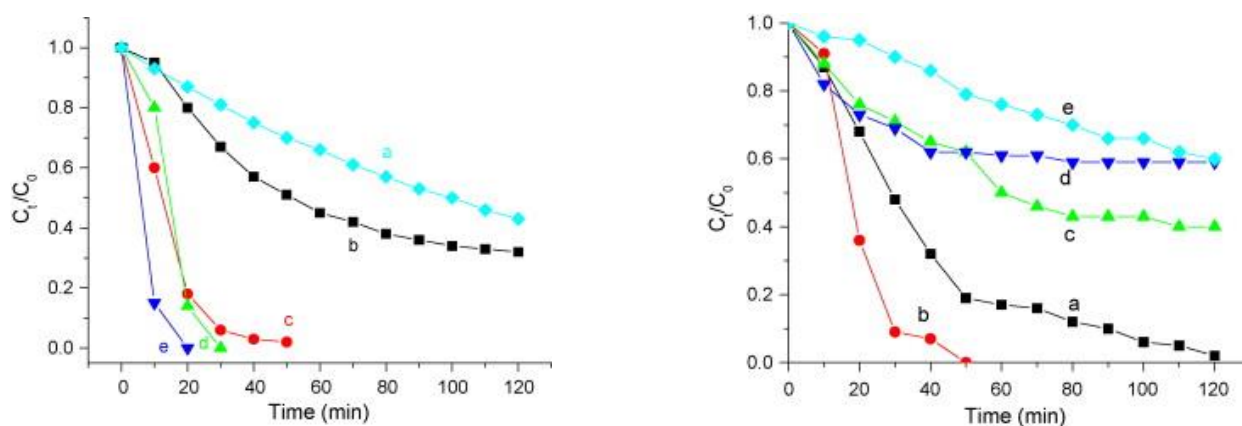
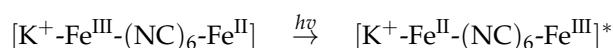


**Figure 7.** (Left): Degradation curves of RhB at different concentrations of potassium chloride under initial conditions:  $1 \times 10^{-4}$  M PB +  $1 \times 10^{-3}$  M  $\text{H}_2\text{O}_2$  +  $4.8 \text{ mg L}^{-1}$  RhB + KCl; (a) 0.0 M KCl; (b) 0.10 M KCl; (c) 0.25 M KCl; (d) 0.50 M KCl; (e) 1.00 M KCl. (Right): Degradation curves of  $4.8 \text{ mg/L}$  RhB containing  $2 \times 10^{-4}$  M PB +  $2 \times 10^{-3}$  M  $\text{H}_2\text{O}_2$ , with (a) no salinity, (b) 0.2 M KCl added, (c) 0.2 M NaCl added, (d) 0.2 M RbCl added, and (e) 0.2 M CsCl added. Reprinted from Ref. [50], with permission from Elsevier.

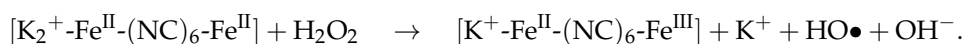
The authors pushed their study further by adding other chloride salts (KCl, NaCl, RbCl, and CsCl) to the reaction mixture, observing another two facts: (1) KCl is the best choice to promote RhB degradation; (2) the degradation amount followed the series of cations of group I. By coupling these observations with electrochemical analyses, the authors could draw some interesting conclusions about the reaction mechanism, which are of general value regarding the use of PB in photo-Fenton processes. These conclusions are: (i) the photocatalytic reaction also takes place inside the PB particles (the reader should bear in mind that PB has zeolitic-like channels of  $3.2 \text{ \AA}$  in diameter); (ii) the initial reaction of the photo-Fenton process is:



which represents the photo-driven intervalence charge transfer. The excited PB nanoparticles are metastable and can oxidize  $\text{H}_2\text{O}_2$  to release dioxygen. Thus, the second step reaction should be:



wherein the latter complex is Prussian white, which then transforms hydrogen peroxide into hydroxyl radicals:



One can see the potassium ions enter and exit the PB particles as counterions.

This function of molecular recognition can be exploited to design catalysts with enhanced performance.

Singh and Pandey prepared PB nanoparticles, tuning the crystalline sizes to between 13 and 53 nm, and tested them in photo-Fenton reactions, using natural UV and simulated solar light to degrade RhB [51]. PB nanoparticles were prepared by mixing iron ferricyanide with 2-(3,4-epoxycyclohexyl)ethyltrimethoxysilane (EETMSi) as a reductive agent and cyclohexanone at 333 K. Different degradation conditions were explored: different room temperatures, solar light irradiation, UV light, and increasing the reaction temperature at 333 K, with RhB concentrations from 10 to 50 ppm. They recorded degradation performances that increased with a reduction in crystalline sizes. Most importantly, they tested their catalysts using polluted river water containing interfering substances such as sulfate, carbonate, and bicarbonate ions and some organics, demonstrating the effectiveness of PB, even in these rather harsh conditions.

PMS activation by PBAs was tested against RhB by Ai et al. [52]. They used in situ synthesis to prepare Co-Fe PBA on a zeolitic imidazolate framework-8 (ZIF-8), obtaining PBA nanocrystals with a diameter of a few tens of nanometers on 150 nm ZIF-8. RhB degradation was investigated under different conditions by changing the PMS concentration, catalyst dosage, the pH of the reaction solution, and NaCl concentration. Prior to light irradiation, the systems were allowed to reach adsorption-desorption equilibrium for 1 h. The authors achieved fairly good RhB degradation in 30 min with a PMS concentration higher than 100 ppm.

### 3.2. Removal of Pharmaceuticals

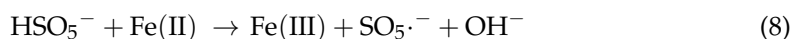
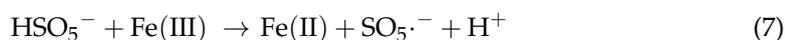
Most investigations presenting the degradation of pharmaceuticals catalyzed by PBAs are based on sulfate activation.

Zeng et al. studied the degradation of carbamazepine by PBAs incorporated in interlayers of layered double hydroxides via peroxymonosulfate (PMS) activation [53].

Levofloxacin hydrochloride (LVF) was treated with Co-Fe PBA deposited on reduced graphene oxide by Pi et al. [54]. The choice of materials was motivated by the acknowledged capability of copper to activate peroxisulfate [55].

Magnetic Co-Fe PBA@RGO was prepared by a two-step hydrothermal method. Morphological analysis (Figure 8) evidenced a certain degree of agglomeration for pure Co-Fe PBA, featuring particles with an average diameter of around 20 nm; instead, dispersion of the RGO surface could ensure uniformly dispersed Co-Fe PBA particles, which showed, however, an increased diameter of up to 60 nm. The presence of thin-shelled structures was also detected. Catalytic activity against LVF was tested by using 5 mg of catalyst and 20 ppm of LVF in water with 0.1 g/L of peroximonosulfate. The reaction course was monitored through HPLC and TOC. The hybrid composite of Co-Fe PBA@RGO was not active in LVF degradation without the presence of peroximonosulfate, the presence of which drastically supported the reaction; an almost complete removal (97.6%) of LVF was observed in about 30 min. The critical dosage of peroximonosulfate was found to be 1 mM, and pH modulation was also found to affect the degradation capability shown by the catalytic mixture. The authors described the activation of peroxomonosulfate by the concomitant action of the Co(II) and Fe(III) species present on the catalyst surface to produce  $\text{SO}_4\cdot^-$ , as follows:





A pseudo-first-order kinetic model was used to fit the obtained data.

It should be observed that the leaching of both Fe and Co ions was reported, although this was in quantities that still complied with the limits imposed by the law.

An interesting study was conducted by Xiao et al., who doped ceria with PB and tested the composite material in the context of the degradation of norfloxacin (NOR), an antibiotic belonging to the class of fluoroquinolones, in a photo-Fenton process [56]. PB was generated on the surface of  $\text{CeO}_2$  by a wet chemistry approach. The idea behind the use of PB as a doping agent for ceria relied on the assumption that PB could enhance the widely acknowledged photocatalytic skills of  $\text{CeO}_2$ , based on the redox couple  $\text{Ce}^{3+}/\text{Ce}^{4+}$  and on the presence of oxygen vacancies in the lattice, which can trap photogenerated electrons and release photogenerated holes.

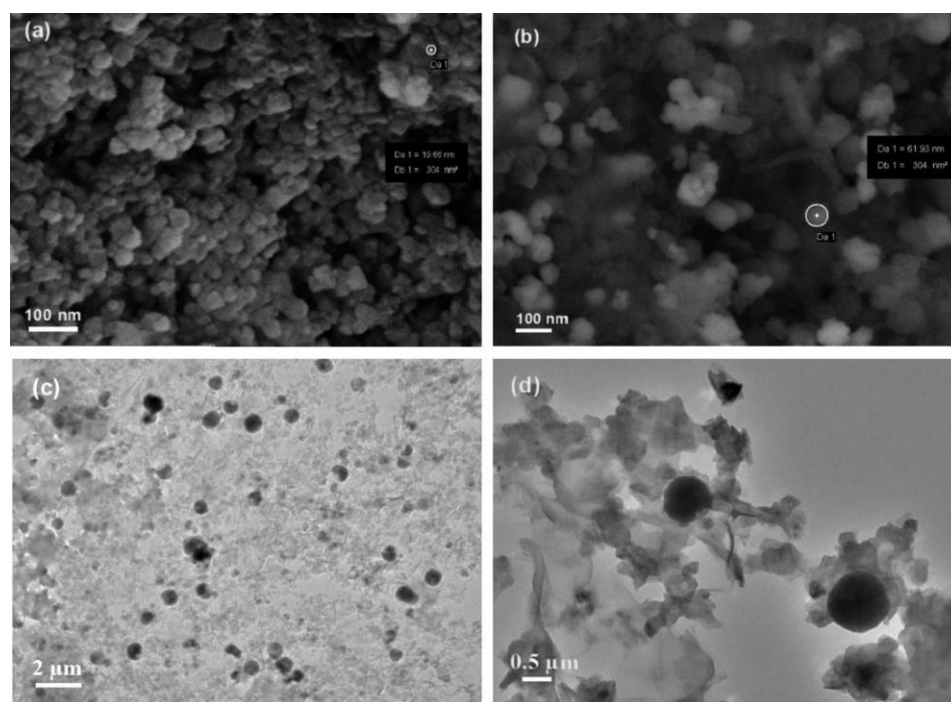


**Figure 8.** SEM images of (a)  $\text{Co}_3[\text{Fe}(\text{CN})_6]_2$  and (b) Co-Fe PBAs@rGO; (c,d) TEM images of Co-Fe PBAs@rGO. Reprinted from Ref. [55], with permission from Elsevier.

NOR degradation was investigated by using 30 mg of catalyst in a 50 mL NOR water solution (16 ppm) in the presence of 5 mL of  $\text{H}_2\text{O}_2$  (6%); after 60 min in the dark, the reaction mixture was irradiated with UV light. NOR degradation and the leaching of iron ions were assessed by UPLC and ICP, respectively. The activity of the ceria was remarkable when hydrogen peroxide was added to the reaction mixture (80% of NOR degraded in 10 min), and was observed to increase upon surface modification with PB (>90% of NOR degraded in 10 min). However, we should notice that no error bars were reported in the plots of the course reaction, making the comparison between the two catalysts slightly unsure. It is important that the reader is aware that this criticism can be applied to the vast majority of the published investigations and, in the view of the author of this review, constitutes an issue that should be addressed. Different mass ratios of PB: $\text{CeO}_2$  resulted

in important differences in the capability of the hybrid catalyst to degrade NOR, with the most effective system containing 10% PB.

The different yields of hydroxyl radicals in the photo-Fenton process were analyzed by electron paramagnetic spectroscopy (EPR). This technique can be extremely useful in the monitoring of processes when radicals are involved and, in this specific case, could provide an important insight into the reaction mechanics. The EPR outcomes showed a higher production of hydroxyl radicals in the PB/CeO<sub>2</sub> system, compared to that observed for bare ceria and for a system of PB + CeO<sub>2</sub>. Indications of cumulative •OH were also found. Furthermore, hydroxyl radicals could be established as the main ROS involved in NOR degradation, with a relatively low contribution from •O<sub>2</sub><sup>−</sup>.

Tetracycline (TC) degradation was catalyzed by a Co-Fe PBA loaded on nickel foam by means of peroxymonosulfate activation by Jin [57]. Co-Fe PBA nanoparticles were deposited in situ on nickel foam, a highly conductive substrate, using different Co:Fe ratios. PBA nanoparticles that were fairly homogeneous in size and shape were detected on the nickel foam surface, together with a homogeneous distribution of Co and Fe (Figure 9).

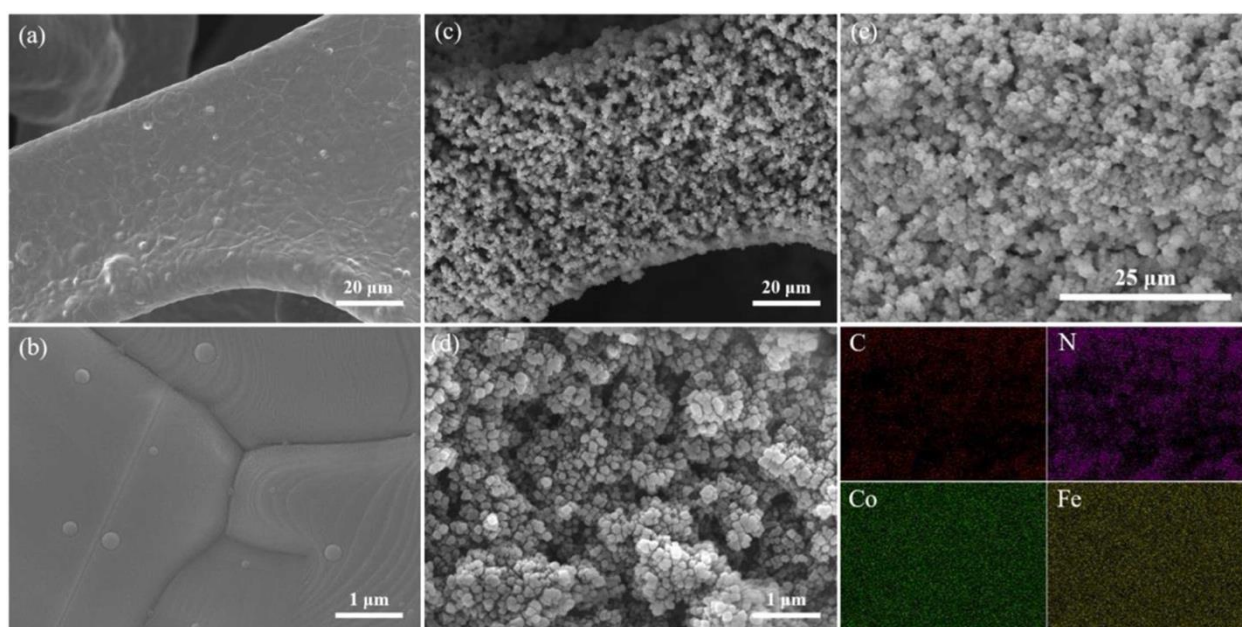


**Figure 9.** SEM images of (a,b) pure NF and (c,d) CoFe-PBA/NF-2.0; (e) elemental mapping images of CoFe-PBA/NF-2.0. Reprinted from Ref. [57], with permission from Elsevier.

Catalytic activity was tested against a 20 ppm TC solution, evaluating different parameters such as PBA nature (ratio Co:Fe), different PMS amounts (Figure 10a), initial TC concentration (Figure 10b), acidic or basic pH (Figure 10c), and the presence of inorganic anions (Figure 10d). When the reaction conditions were properly adjusted, a fairly good degradation level of TC was recorded in 30 min.

The Co:Fe ratio was also found to play an important role: the higher the cobalt content, the higher the TC degradation, highlighting the role of this metal ion in spurring PMS activation, as previously observed.

A quenching experiment and EPR were used to analyze the active species involved in TC degradation, indicating that four ROS were involved: SO<sub>4</sub><sup>•−</sup>, •OH, O<sub>2</sub><sup>•−</sup>, and <sup>1</sup>O<sub>2</sub>, produced by peroxymonosulfate activation by Co-Fe PBA. Ni<sup>2+</sup> ions belonging to nickel foam were also assumed to take part in the activation process.

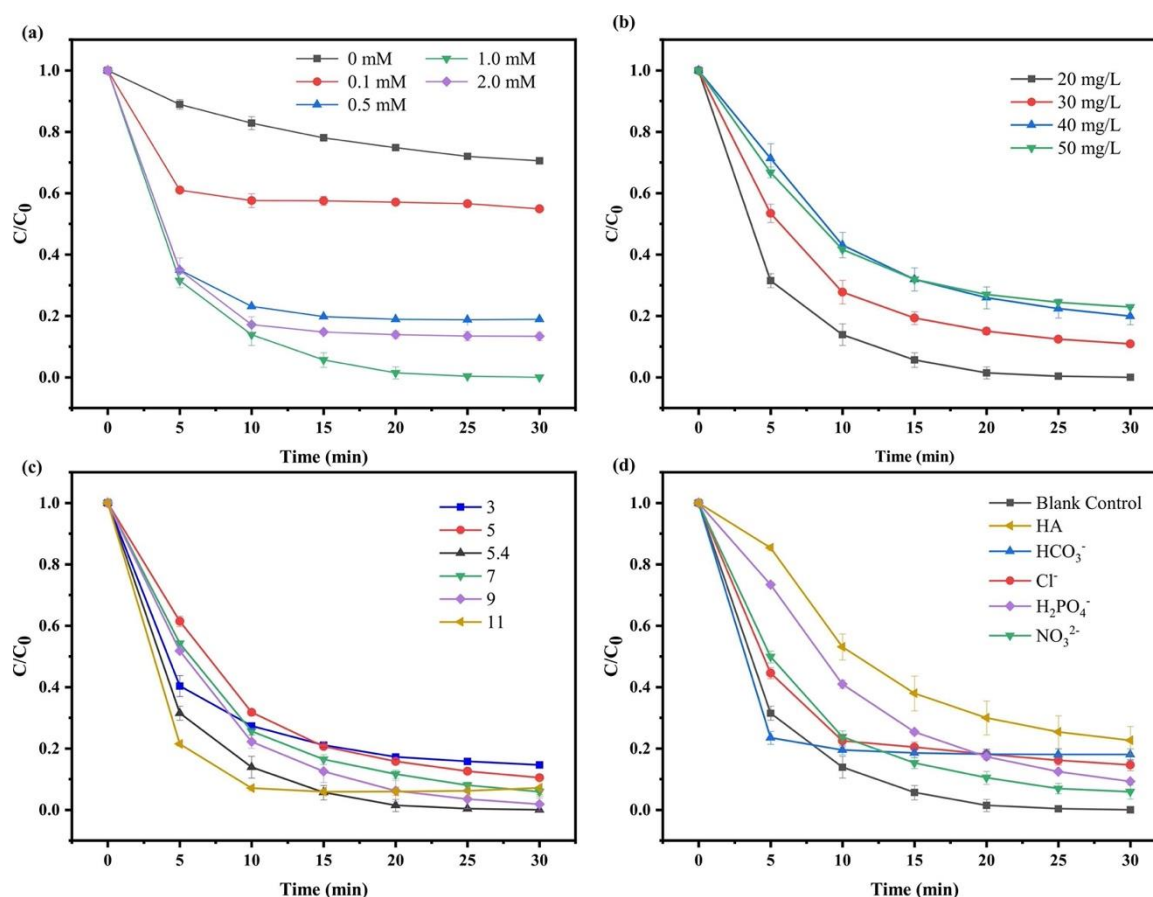


**Figure 10.** The effects of (a) PMS dosages, (b) initial TC concentrations, (c) pH values, and (d) inorganic anions and NOM. Reprinted from Ref. [57], with permission from Elsevier.

Kahsevani et al. compared the performance of four PBAs (PB, Cu-PBA, Co-PBA, and Mn-PBA) in the catalytic degradation of ciprofloxacin (CIP) [58], another antibiotic in the class of fluoroquinolones. Catalytic tests explored the skill of PBAs at removing and degrading CIP (10 ppm) without any supporting chemical. They found that all the PBAs are active catalysts under dark conditions, with a removal rate higher than 30% of the initial CIP amount in 3 h of reaction time (with the exception of CoPBA, which could remove less than 10%). Simulated solar light irradiation spurred the reaction, with about 80% of the initial CIP degraded in 2 h by Co-PBA and Mn-PBA (while both PB and Cu-PBA did not surpass 32%). The interest offered by this work relies on two aspects analyzed by the authors. The first point is that they observed a kinetic order higher than first under dark conditions and an auto-catalytic reaction when the system was subjected to light irradiation after the dark period (which confirmed that the degradation of the pharmaceutical under dark conditions was not pure adsorption), as shown in Figure 11. The second interesting aspect concerned the deep FTIR analysis of the materials before and after light irradiation, which highlighted a significant change in the Fe(II)/Fe(III) ratio. The authors hypothesized a spin crossover, favoring a high spin status, which should then spur on the catalytic activity. The catalytic activity, and the differences observed among the investigated batch, were discussed from a coordination chemistry viewpoint, hypothesizing the formation of a five- or six-membered complex between the organic target and the PBAs.

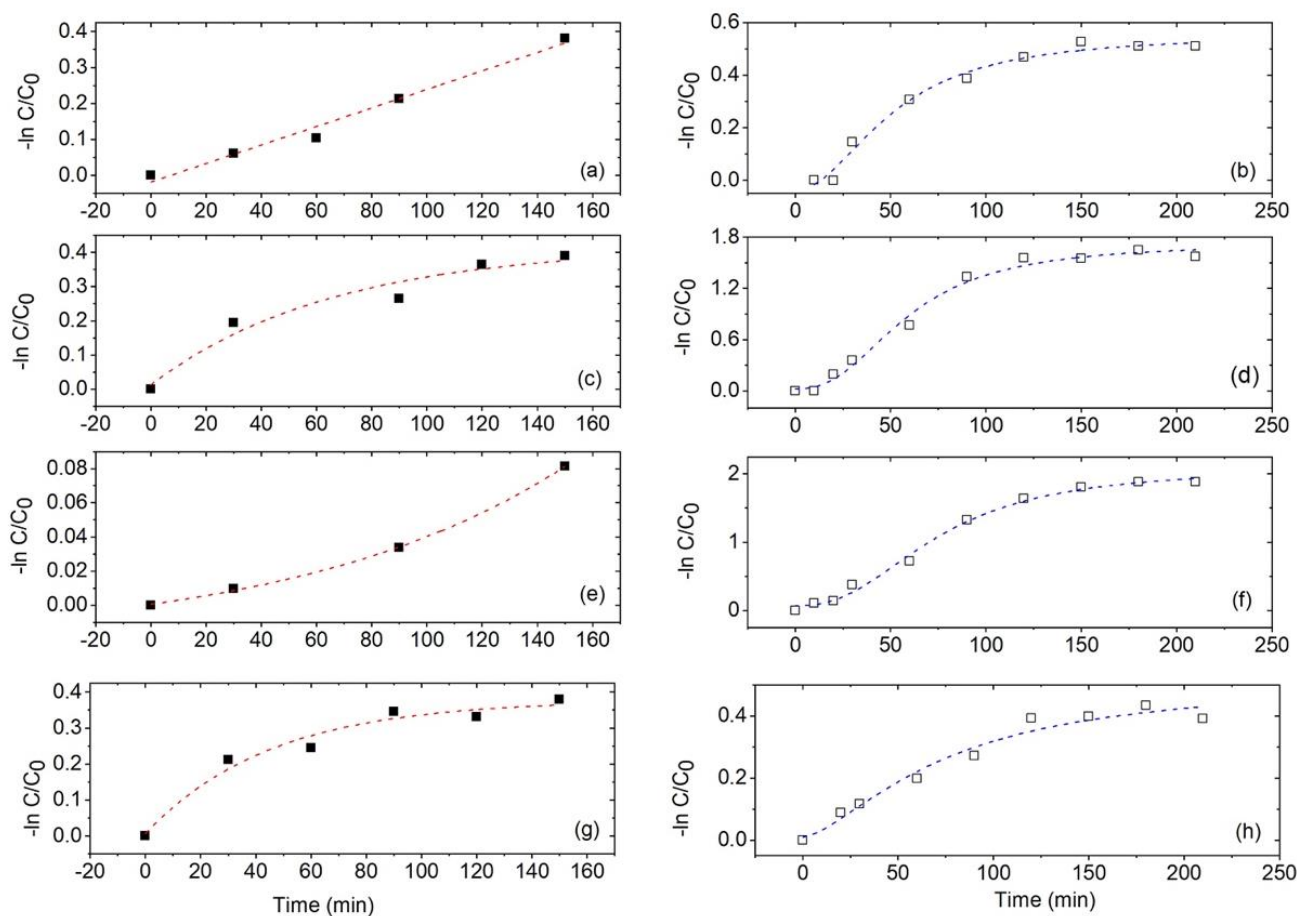


**Figure 11.** Semilog plots of the CIP degradation reaction monitored under dark conditions (a,c,e,g) and upon light irradiation following the dark period (b,d,f,h). (a,b): FeHCF; (c,d): MnHCF; (e,f) CoHCF; (g,h) CuHCF. The markers are experimental points and the lines are fitting curves. Reprinted from Ref. [58].

### 3.3. Removal of Phenol

Gögen et al. synthesized magnetic PB on multi-walled CNTs to degrade phenol through a Fenton process [59]. The magnetite nanoparticles, modified in situ with PB, displayed a spherical shape with an average diameter as high as 170 nm and could be well dispersed in the CNTs matrix (Figure 12). XPS analysis showed the presence on the surface of composites of both  $\text{Fe}_3\text{O}_4$  and PB.

The prepared composite showed a good performance, degrading 100% of 50 ppm phenol solution in 60 min, with obvious differences among the tests depending on the catalyst used and the  $\text{H}_2\text{O}_2$  amounts. Good recyclability was also observed. It should, however, be remarked that: (i) both CNTs and magnetite particles are active as photo-Fenton catalysts in the removal of phenol (even though the magnetite action was sped up by the presence of PB); (ii) the difference in performance between the PB-modified magnetite nanoparticles and the hybrid composite with CNTs was not very relevant for long reaction times (60 min), which poses doubts as to the real need for CNTs.

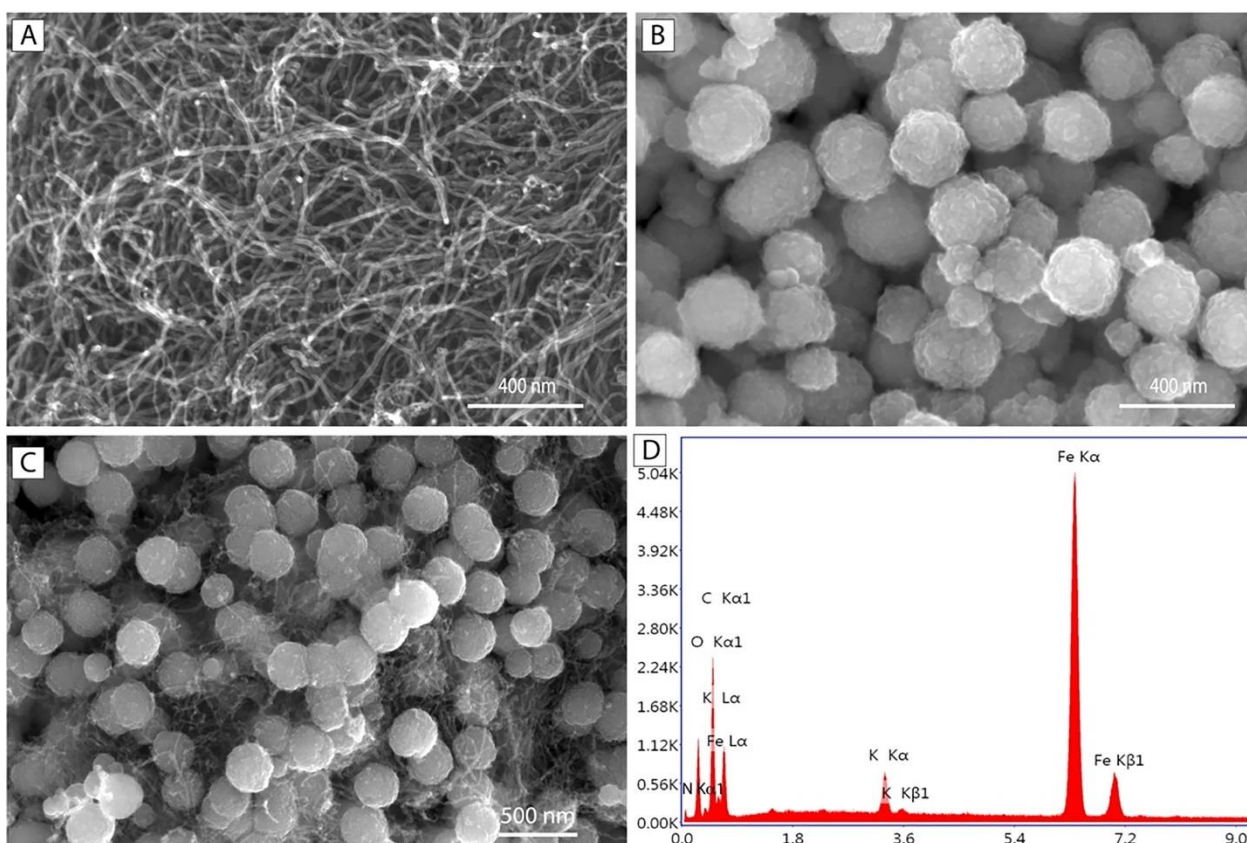


**Figure 12.** SEM images of (A) MW-CNT; (B) magnetite nanoparticles modified with Prussian blue (PMM); (C) PMM-CNT; (D) the EDX spectrum of PMM-CNT. Reprinted from Ref. [59], with permission from Springer.

#### 4. Synthesis of Chemicals

The transesterification of  $\beta$ -ketoesters (ethylacetoacetate) with different alcohols was accelerated by PB [60]. The authors hypothesized the formation of five-membered intermediates between PB (the  $\text{Fe}^{\text{III}}$  center) and the ketoester.

CoFe-PBA nanoparticles (about 50 nm) were loaded on carbon nanotubes (CNTs) by Wang and were used to promote the epoxidation of styrene [61]. The CNTs were intended as the catalyst carrier and were devoted to increasing the overall surface area and particle dispersion. The epoxidation of styrene was carried out in the presence of 70% *t*-butyl hydroperoxide. The experimental outcomes showed a higher conversion to the desired product (80% converted styrene, with a selectivity of 62% to styrene oxide) when the hybrid material was used, compared to what was observed when supporting the reaction with either CNTs (47% conversion, with 7% selectivity) or the CoFe PBA nanoparticles standing alone (67% conversion, with a selectivity of 25%). Kinetic studies showed a first-order reaction with respect to the concentrations of the catalyst, styrene, and *t*-butyl hydroperoxide.

The catalytic epoxidation of styrene with *tert*-butyl hydroperoxide (TBPH), promoted by Cu-Co PBA, was also investigated by Liang et al. [62]. After optimization of the reaction parameters, the authors found a 96% conversion of styrene, with selectivity toward styrene epoxide that was as high as 64%, and a first-order reaction with respect to the concentrations of styrene, TBHP, and the catalyst was observed. The proposed mechanism consisted of a reaction between the active metals in the PBA with the TBHP to form a hydroperoxyl compound (pre-equilibrium step), which then lost a *t*-butanol to form an oxometal radical. The latter interacted with styrene, forming a metalloepoxy intermediate, which decomposed to provide the reaction product and give back the PBA.

A ternary catalytic system consisting of sequential electrodeposition on graphene sheets of PB and Pt nanoparticles was exploited to speed up the electrochemical oxidation

of methanol by Wang et al. [63]. In this hybrid system, PB was thought to act as a porous support, enabling both better Pt nanoparticle quality during their electrodeposition and a larger area of these being exposed to the reaction medium. More importantly, according to the authors, PB could also facilitate electron transfer for the oxidative removal of CO (Figure 13), but no experimental proof was shown to support this claim.

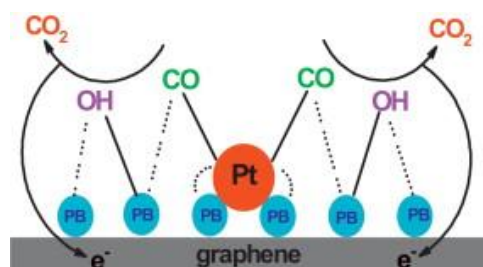


**Figure 13.** Schematic diagram of the possible mechanism for the enhanced performance of PB and Pt nanoparticles electrodeposited on graphene sheets for CO oxidation. Reprinted from Ref. [63], with permission from Elsevier.

Methanol oxidation, as promoted by a series of binary PBAs (NiFe, CuFe, CoFe, and FeFe) on nickel foam, was also investigated by Zhang et al. [64]. Different performances in terms of Faraday efficiency (FE) were found, depending on the specific PBAs, with particularly good FE performance (94.1% at a current density of  $500 \text{ mA cm}^{-2}$ ) being shown by the NiFe PBAs. Spurred by this good achievement, the authors also tested other nucleophilic oxidation reactions (to oxidize ethanol, glycerol, and glucose to their corresponding carboxylates) that were aimed at valorizing biomasses. Their good findings were attributed to the low electron density featured by the NiFe PBA, which can replace the oxygen evolution reaction at the anode, thereby generating value-added chemicals.

The nitration of organic compounds catalyzed by PB in the presence of small amounts of nitric acid under conventional and non-conventional (sonication and microwave irradiation) conditions was reported by Pasnoori et al. [65]. The authors found that the nitration reaction (substrates: salicylic acid, benzonitrile, benzamide, benzoic acid, and benzaldehyde) proceeded smoothly, with very good yields (>80%) and high regioselectivity upon the investigated reaction conditions, but they could not suggest any possible mechanism.

A very interesting investigation was proposed by Marquez and coworkers, who investigated a series of hexacyanocobaltate PBAs for the selective synthesis of propargylamines through  $A^3$  coupling [66]. The authors prepared PBAs featuring the main unit of hexacyanocobaltate and, as the secondary transition metals, Fe, Co, Ni, Cu, and Zn. They found variations in the reaction outcomes, depending on the nature of the secondary transition metal (Figure 14), with a particularly good performance shown by the ternary PBA CuZn-Co. They proposed a reaction mechanism based on the coordination capability of the PBAs toward the functional groups of the reactants (either a carboxylic acid or a triple carbon bond). This work highlights the importance of the proper choice of PBA composition in catalysis: the reported outcomes agreed with previous literature findings on the catalytic activity of Cu sites for the same kind of reaction, while, when a Fe-Co PBA was employed, disappointing results were reported, even though the use of iron as a catalytic site had been previously suggested as effective.

A series of PBAs was investigated by Zheng et al. for the aerobic oxidation of vanillyl alcohol (VAL) to vanillin (VN), a valuable product used in several industries [67]. The authors prepared several PBAs in the form of  $M^{II}_3[M^{III}(CN)_6]_2$ , where  $M^{II} = \text{Mn, Fe, Co, Ni, Cu, Zn}$ , and  $M^{III} = \text{Fe, Co}$ , using the coprecipitation approach. Oxygen gas was used as the oxidizing agent. PB was evaluated to be the best catalyst of the batch, with a yield (47%) and selectivity (>99%) higher than those provided by its analogues. In the presence of gaseous  $O_2$ , it is assumed that the metal complex directly reacts with the molecular

oxygen to generate a metallic superoxo complex, which can generate a hydroxyl radical by detaching the –OH functional group from the vanillic acid, starting the conversion process.

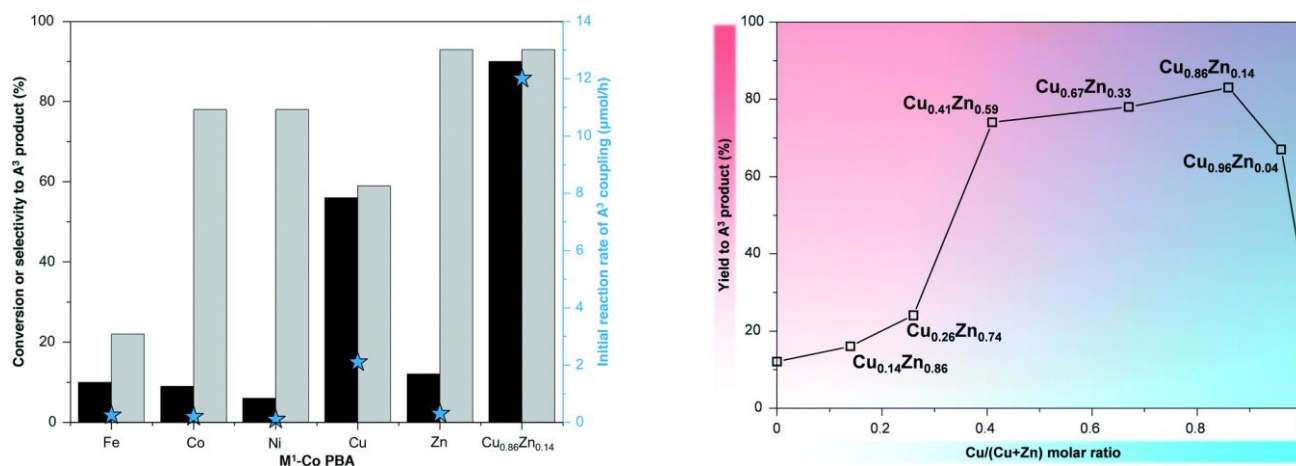


**Figure 14.** (Left): Conversion (black bars) and selectivity (grey bars) for the A<sup>3</sup> product for the coupling of phenylacetylene (0.05 mmol), piperidine (0.1 mmol), and benzaldehyde (0.1 mmol) after 24 h of reaction time at 383 K and the initial rate (star) of the A<sup>3</sup> coupling, expressed as μmol of the A<sup>3</sup> product formed per h over 10 mg of PBA. Conversion and selectivity are based on phenylacetylene. (Right) Yield of the A<sup>3</sup> product after 24 h of reaction time for the coupling of phenylacetylene (0.05 mmol), piperidine (0.1 mmol), and benzaldehyde (0.1 mmol) at 383 K over 10 mg of Cu<sub>x</sub>Zn<sub>1-x</sub>-Co PBA with different Cu/(Cu + Zn) molar ratios. Reprinted from Ref. [66].

## 5. Conclusions and Criticisms

PB and its analogues deserve their renaissance: they are valuable materials in catalysis and hold potential for both chemical synthesis and pollutant degradation. However, these two applications constitute a niche field in their use (their application as energy-storing materials is more widely investigated) and the current knowledge is worthy of being extended.

A critical point to highlight is the difficulty of reliably comparing the literature outcomes: different experimental conditions make this operation a real challenge. This can be problematic in view of moving from lab-scale tests to real-life applications.

An example of this is that few works allow the reader to actually get the full picture of PBA composition, which, as briefly discussed in the introduction, plays a great role in determining their performance. Their possible changes after being used in catalytic processes are also seldom analyzed; reporting their recyclability, as important as it can be from an application viewpoint, is not enough to fully understand this class of materials. Experimental differences hindering a common effort toward the fabrication of reliable catalysts also rely on the use of different conditions in terms of: (i) the concentration of the target pollutant; (ii) the concentration of redox supporters (hydrogen peroxide and sulfate); (iii) light irradiation (light energy and power) when used. The setup of standard protocols for an investigation of the catalytic ability of new materials is seen as mandatory if real progress in the field is pursued.

Furthermore, in many cases, the reaction mechanisms are not unveiled. This impairs progress in catalyst design, which is a shame for a class of materials that can be tailored almost at will. Analysis of the literature results also poses questions about the analysis of reaction kinetics: almost always, the researchers choose to forcibly apply a pseudo-first-order kinetic model, even when faced with data that cannot be linearized. This is not acceptable, and more effort is needed in the decryption of the actual process kinetics.

In all the cases presented in this review, PBAs are used as heterogeneous catalysts, but few studies investigated the leaching of metals during the catalytic reactions or the possible partial dissolution of the materials, which would result in a mixed heterogeneous-

homogeneous catalytic process. This aspect should be addressed: if the scientific community really aims to achieve the use of PBAs in real-world catalytic applications, it must make sure that: (i) no further contamination of water is induced during the catalytic removal of pollutants; (ii) no unwanted residuals are present in the products of PBA-sustained catalytic chemical synthesis. Moreover, the potential occurrence of homogeneous catalysis poses doubts as to the actual reaction mechanisms and the real role of PBAs.

While the investigation of common dyes, such as Rhodamine B and Methyl Orange, is still useful for a quick check of the catalytic potential of PBAs, this habit is not enough to prove their actual potential. As herein reported, the study of the degradation of antibiotics has shown interesting results, but the number of scientific papers in this specific field is still quite low, while the topic definitely deserves more attention, with water contamination from antibiotic residues being an emerging major issue.

Last, but not least, the use of in situ and/or operando analytical techniques, the development of which is facing a rapid increase, seems mandatory for deepening our understanding of the changes in materials induced by operating conditions, as well as of timescales of these changes.

Despite these limits, or maybe thanks to them, the field of Prussian blue analogues as catalysts has considerable room for development, which can, on the one hand, lead to the fabrication of efficient catalysts and, on the other hand, deepen our understanding of this fascinating class of materials.

**Funding:** The Author would like to acknowledge Luleå University of Technology (LTU) for partial funding, under the Project SUPERCAP (LTU Jubilee Fund).

**Data Availability Statement:** No new data were created or analyzed in this study. Data sharing is not applicable to this article.

**Conflicts of Interest:** The Author declares no conflict of interest.

## References

1. Paolella, A.; Faure, C.; Timoshevskii, V.; Marras, S.; Bertoni, G.; Guerfi, A.; Vijh, A.; Armand, M.; Zaghbi, K. A Review on Hexacyanoferrate-Based Materials for Energy Storage and Smart Windows: Challenges and Perspectives. *J. Mater. Chem. A* **2017**, *5*, 18919–18932. [CrossRef]
2. Yu, Z.Y.; Duan, Y.; Liu, J.D.; Chen, Y.; Liu, X.K.; Liu, W.; Ma, T.; Li, Y.; Zheng, X.S.; Yao, T.; et al. Unconventional CN Vacancies Suppress Iron-Leaching in Prussian Blue Analogue Pre-Catalyst for Boosted Oxygen Evolution Catalysis. *Nat. Commun.* **2019**, *10*, 2799. [CrossRef] [PubMed]
3. Ulusoy Ghobadi, T.G.; Ozbay, E.; Karadas, F. How to Build Prussian Blue Based Water Oxidation Catalytic Assemblies: Common Trends and Strategies. *Chem. Eur. J.* **2021**, *27*, 3638–3649. [CrossRef]
4. Prussian Blue. Available online: <https://www.acs.org/molecule-of-the-week/archive/p/prussian-blue.html> (accessed on 15 April 2024).
5. Bornamehr, B.; Presser, V.; Zarbin, A.J.G.; Yamauchi, Y.; Husmann, S. Prussian Blue and Its Analogues as Functional Template Materials: Control of Derived Structure Compositions and Morphologies. *J. Mater. Chem. A* **2023**, *11*, 10473–10492. [CrossRef]
6. Du, G.; Pang, H. Recent Advancements in Prussian Blue Analogues: Preparation and Application in Batteries. *Energy Storage Mater.* **2021**, *36*, 387–408. [CrossRef]
7. Ying, S.; Chen, C.; Wang, J.; Lu, C.; Liu, T.; Kong, Y.; Yi, F.-Y. Synthesis and Applications of Prussian Blue and Its Analogues as Electrochemical Sensors. *Chempluschem* **2021**, *86*, 1608–1622. [CrossRef] [PubMed]
8. Huang, Y.; Ren, S. Multifunctional Prussian Blue Analogue Magnets: Emerging Opportunities. *Appl. Mater. Today* **2021**, *22*, 100886. [CrossRef]
9. Yue, Y.; Zhang, Z.; Binder, A.J.; Chen, J.; Jin, X.; Overbury, S.H.; Dai, S. Hierarchically Superstructured Prussian Blue Analogues: Spontaneous Assembly Synthesis and Applications as Pseudocapacitive Materials. *ChemSusChem* **2015**, *8*, 177–183. [CrossRef]
10. Cao, L.-M.; Lu, D.; Zhong, D.-C.; Lu, T.-B. Prussian Blue Analogues and Their Derived Nanomaterials for Electrocatalytic Water Splitting. *Coord. Chem. Rev.* **2020**, *407*, 213156. [CrossRef]
11. Dong, X.; Liu, X.; Cheng, M.; Huang, D.; Zhang, G.; Wang, W.; Du, L.; Wang, G.; Liu, H. Prussian Blue and Its Analogues: Reborn as Emerging Catalysts for a Fenton-like Process in Water Purification. *Coord. Chem. Rev.* **2023**, *482*, 215067. [CrossRef]
12. Li, W.J.; Han, C.; Cheng, G.; Chou, S.L.; Liu, H.K.; Dou, S.X. Chemical Properties, Structural Properties, and Energy Storage Applications of Prussian Blue Analogues. *Small* **2019**, *15*, 1900470. [CrossRef] [PubMed]
13. Itaya, K.; Shoji, N.; Uchida, I. Catalysis of the Reduction of Molecular Oxygen to Water at Prussian Blue Modified Electrodes. *J. Am. Chem. Soc.* **1984**, *106*, 3423–3429. [CrossRef]

14. Xuan, C.; Zhang, J.; Wang, J.; Wang, D. Rational Design and Engineering of Nanomaterials Derived from Prussian Blue and Its Analogs for Electrochemical Water Splitting. *Chem. Asian J.* **2020**, *15*, 958–972. [[CrossRef](#)] [[PubMed](#)]
15. Zhang, G.; Li, Y.; Xiao, X.; Shan, Y.; Bai, Y.; Xue, H.-G.; Pang, H.; Tian, Z.; Xu, Q. In Situ Anchoring Polymetallic Phosphide Nanoparticles within Porous Prussian Blue Analogue Nanocages for Boosting Oxygen Evolution Catalysis. *Nano Lett.* **2021**, *21*, 3016–3025. [[CrossRef](#)] [[PubMed](#)]
16. Su, X.; Wang, Y.; Zhou, J.; Gu, S.; Li, J.; Zhang, S. Operando Spectroscopic Identification of Active Sites in NiFe Prussian Blue Analogues as Electrocatalysts: Activation of Oxygen Atoms for Oxygen Evolution Reaction. *J. Am. Chem. Soc.* **2018**, *140*, 11286–11292. [[CrossRef](#)] [[PubMed](#)]
17. Alsaç, E.P.; Ülker, E.; Nune, S.V.K.; Dede, Y.; Karadas, F. Tuning the Electronic Properties of Prussian Blue Analogues for Efficient Water Oxidation Electrocatalysis: Experimental and Computational Studies. *Chem. Eur. J.* **2018**, *24*, 4856–4863. [[CrossRef](#)]
18. Meng, X.; Yang, J.; Zhang, C.; Fu, Y.; Li, K.; Sun, M.; Wang, X.; Dong, C.; Ma, B.; Ding, Y. Light-Driven CO<sub>2</sub> Reduction over Prussian Blue Analogues as Heterogeneous Catalysts. *ACS Catal.* **2022**, *12*, 89–100. [[CrossRef](#)]
19. Lee, J.H.; Kattel, S.; Wang, Y.; Tackett, B.M.; Xie, Z.; Hwang, S.; Denny, S.R.; Xu, W.; Chen, J.G. Prussian Blue Analogues as Platform Materials for Understanding and Developing Oxygen Evolution Reaction Electrocatalysts. *J. Catal.* **2021**, *393*, 390–398. [[CrossRef](#)]
20. Stohl, A.; Seibert, P.; Wotawa, G.; Arnold, D.; Burkhart, J.F.; Eckhardt, S.; Tapia, C.; Vargas, A.; Yasunari, T.J. Xenon-133 and Caesium-137 Releases into the Atmosphere from the Fukushima Dai-Ichi Nuclear Power Plant: Determination of the Source Term, Atmospheric Dispersion, and Deposition. *Atmos. Chem. Phys.* **2012**, *12*, 2313–2343. [[CrossRef](#)]
21. Awual, M.R.; Suzuki, S.; Taguchi, T.; Shiwaku, H.; Okamoto, Y.; Yaita, T. Radioactive Cesium Removal from Nuclear Wastewater by Novel Inorganic and Conjugate Adsorbents. *Chem. Eng. J.* **2014**, *242*, 127–135. [[CrossRef](#)]
22. Awual, M.R.; Yaita, T.; Taguchi, T.; Shiwaku, H.; Suzuki, S.; Okamoto, Y. Selective Cesium Removal from Radioactive Liquid Waste by Crown Ether Immobilized New Class Conjugate Adsorbent. *J. Hazard. Mater.* **2014**, *278*, 227–235. [[CrossRef](#)] [[PubMed](#)]
23. Kotilainen, A.T.; Kotilainen, M.M.; Varti, V.P.; Hutri, K.L.; Virtasalo, J.J. Chernobyl Still with Us: 137Caesium Activity Contents in Seabed Sediments from the Gulf of Bothnia, Northern Baltic Sea. *Mar. Pollut. Bull.* **2021**, *172*, 112924. [[CrossRef](#)] [[PubMed](#)]
24. Ishizaki, M.; Akiba, S.; Ohtani, A.; Hoshi, Y.; Ono, K.; Matsuba, M.; Togashi, T.; Kananizuka, K.; Sakamoto, M.; Takahashi, A.; et al. Proton-Exchange Mechanism of Specific Cs<sup>+</sup> Adsorption via Lattice Defect Sites of Prussian Blue Filled with Coordination and Crystallization Water Molecules. *Dalt. Trans.* **2013**, *42*, 16049–16055. [[CrossRef](#)] [[PubMed](#)]
25. Thammawong, C.; Opaprakasit, P.; Tangboriboonrat, P.; Sreearunothai, P. Prussian Blue-Coated Magnetic Nanoparticles for Removal of Cesium from Contaminated Environment. *J. Nanoparticle Res.* **2013**, *15*, 1689. [[CrossRef](#)]
26. Verzijl, J.M.; Joore, J.C.; van Dijk, A.; Glerum, J.H.; Savelkoul, T.J.; Sangster, B.; van het Schip, A.D. In Vitro Binding Characteristics for Cesium of Two Qualities of Prussian Blue, Activated Charcoal and Resonium-A. *J. Toxicol. Clin. Toxicol.* **1992**, *30*, 215–222. [[CrossRef](#)] [[PubMed](#)]
27. Kim, H.; Wi, H.; Kang, S.; Yoon, S.; Bae, S.; Hwang, Y. Prussian Blue Immobilized Cellulosic Filter for the Removal of Aqueous Cesium. *Sci. Total Environ.* **2019**, *670*, 779–788. [[CrossRef](#)] [[PubMed](#)]
28. Jung, Y.; Choi, U.S.; Ko, Y.G. Securely Anchored Prussian Blue Nanocrystals on the Surface of Porous PAAm Sphere for High and Selective Cesium Removal. *J. Hazard. Mater.* **2021**, *420*, 126654. [[CrossRef](#)]
29. Liu, P.S.; Cui, G.; Guo, Y.J. A Lightweight Porous Ceramic Foam Loading Prussian Blue Analogue for Removal of Toxic Ions in Water. *Mater. Lett.* **2016**, *182*, 273–276. [[CrossRef](#)]
30. Chen, S.; Hu, J.; Guo, Y.; Belzile, N.; Deng, T. Enhanced Kinetics and Super Selectivity toward Cs<sup>+</sup> in Multicomponent Aqueous Solutions: A Robust Prussian Blue Analogue/Polyvinyl Chloride Composite Membrane. *Environ. Res.* **2020**, *189*, 109952. [[CrossRef](#)]
31. Kim, H.; Kim, M.; Kim, W.; Lee, W.; Kim, S. Photocatalytic Enhancement of Cesium Removal by Prussian Blue-Deposited TiO<sub>2</sub>. *J. Hazard. Mater.* **2018**, *357*, 449–456. [[CrossRef](#)]
32. Chen, S.; Yang, X.; Wang, Z.; Hu, J.; Han, S.; Guo, Y.; Deng, T. Prussian Blue Analogs-Based Layered Double Hydroxides for Highly Efficient Cs<sup>+</sup> Removal from Wastewater. *J. Hazard. Mater.* **2021**, *410*, 124608. [[CrossRef](#)] [[PubMed](#)]
33. Huo, J.; Yu, G.; Wang, J. Selective Adsorption of Cesium (I) from Water by Prussian Blue Analogues Anchored on 3D Reduced Graphene Oxide Aerogel. *Sci. Total Environ.* **2021**, *761*, 143286. [[CrossRef](#)] [[PubMed](#)]
34. Li, H.; Zhang, L.; Chen, J.; Lu, M.; Xie, J.; Wang, X.; Han, K.; Li, J.; Lu, J. Reduced Graphene Oxide Based Aerogels: Doped with Ternary Prussian Blue Analogs and Selective Removal of Cs<sup>+</sup> from Effluent. *J. Water Process Eng.* **2022**, *47*, 102741. [[CrossRef](#)]
35. Ferreira-Neto, E.P.; Ullah, S.; Perissinotto, A.P.; de Vicente, F.S.; Ribeiro, S.J.L.; Worsley, M.A.; Rodrigues-Filho, U.P. Prussian Blue as a Co-Catalyst for Enhanced Cr(vi) Photocatalytic Reduction Promoted by Titania-Based Nanoparticles and Aerogels. *New J. Chem.* **2021**, *45*, 10217–10231. [[CrossRef](#)]
36. Moazezi, N.; Moosavian, M.A. Removal of Rubidium Ions by Polyaniline Nanocomposites Modified with Cobalt-Prussian Blue Analogues. *J. Environ. Chem. Eng.* **2016**, *4*, 2440–2449. [[CrossRef](#)]
37. López, Y.C.; Ortega, G.A.; Martínez, M.A.; Reguera, E. Magnetic Prussian Blue Derivative like Absorbent Cages for an Efficient Thallium Removal. *J. Clean. Prod.* **2021**, *283*, 124587. [[CrossRef](#)]
38. Zhang, H.; Qi, J.; Liu, F.; Wang, Z.; Ma, X.; He, D. One-Pot Synthesis of Magnetic Prussian Blue for the Highly Selective Removal of Thallium(I) from Wastewater: Mechanism and Implications. *J. Hazard. Mater.* **2022**, *423*, 126972. [[CrossRef](#)] [[PubMed](#)]

39. Uogintė, I.; Lujanienė, G.; Mažeika, K. Study of Cu (II), Co (II), Ni (II) and Pb (II) Removal from Aqueous Solutions Using Magnetic Prussian Blue Nano-Sorbent. *J. Hazard. Mater.* **2019**, *369*, 226–235. [[CrossRef](#)]
40. Hu, L.; Mei, J.; Chen, Q.; Zhang, P.; Yan, N. Magnetically Separable Prussian Blue Analogue  $Mn_3[Co(CN)_6]_2 \cdot nH_2O$  Porous Nanocubes as Excellent Absorbents for Heavy Metal Ions. *Nanoscale* **2011**, *3*, 4270–4274. [[CrossRef](#)]
41. Zhou, W.Y.; Sun, R.; Li, S.S.; Guo, Y.; Shen, W.; Wang, J.; Deepak, F.L.; Li, Y.; Wang, Z. Engineering Surface Electron and Active Site at Electrochemical Sensing Interface of CN Vacancy-Mediated Prussian Blue Analogue for Analysis of Heavy Metal Ions. *Appl. Surf. Sci.* **2021**, *564*, 150131. [[CrossRef](#)]
42. Zhou, Y.; Xu, N.; Tian, K.; Qing, T.; Hao, Y.; Liang, P.; Li, M. Nitriilotriacetic Acid Modified Magnetic Prussian Blue for Efficient Removal of Cadmium from Wastewater. *Appl. Surf. Sci.* **2022**, *600*, 154102. [[CrossRef](#)]
43. Long, X.; Chen, H.; Huang, T.; Zhang, Y.; Lu, Y.; Tan, J.; Chen, R. Removal of Cd(II) from Micro-Polluted Water by Magnetic Core-Shell  $Fe_3O_4@Prussian\ Blue$ . *Molecules* **2021**, *26*, 2497. [[CrossRef](#)] [[PubMed](#)]
44. Sebti, E.; Besli, M.M.; Metzger, M.; Hellstrom, S.; Schultz-Neu, M.J.; Alvarado, J.; Christensen, J.; Doeff, M.; Kuppen, S.; Subban, C. V Removal of  $Na^+$  and  $Ca^{2+}$  with Prussian Blue Analogue Electrodes for Brackish Water Desalination. *Desalination* **2020**, *487*, 114479. [[CrossRef](#)]
45. Ameta, R.; Chohadia, K.A.; Jain, A.; Punjabi, P.B. Chapter 3—Fenton and Photo-Fenton Processes. In *Advanced Oxidation Processes for Waste Water Treatment*; Ameta, S.C., Ameta, R., Eds.; Academic Press: Cambridge, MA, USA, 2018; pp. 49–87, ISBN 978-0-12-810499-6.
46. Lee, J.; von Gunten, U.; Kim, J.-H. Persulfate-Based Advanced Oxidation: Critical Assessment of Opportunities and Roadblocks. *Environ. Sci. Technol.* **2020**, *54*, 3064–3081. [[CrossRef](#)] [[PubMed](#)]
47. Nossol, E.; Nossol, A.B.S.; Zarbin, A.J.G.; Bond, A.M. Carbon Nanotube/Prussian Blue Nanocomposite Film as a New Electrode Material for Environmental Treatment of Water Samples. *RSC Adv.* **2013**, *3*, 5393–5400. [[CrossRef](#)]
48. Tong, X.; Jia, W.; Li, Y.; Yao, T.; Wu, J.; Yang, M. One-Step Preparation of Reduced Graphene Oxide/Prussian Blue/Polypyrrole Aerogel and Their Enhanced Photo-Fenton Performance. *J. Taiwan Inst. Chem. Eng.* **2019**, *102*, 92–98. [[CrossRef](#)]
49. Li, X.; Wang, J.; Rykov, A.I.; Sharma, V.K.; Wei, H.; Jin, C.; Liu, X.; Li, M.; Yu, S.; Sun, C.; et al. Prussian Blue/ $TiO_2$  Nanocomposites as a Heterogeneous Photo-Fenton Catalyst for Degradation of Organic Pollutants in Water. *Catal. Sci. Technol.* **2015**, *5*, 504–514. [[CrossRef](#)]
50. Liu, S.Q.; Cheng, S.; Feng, L.R.; Wang, X.M.; Chen, Z.G. Effect of Alkali Cations on Heterogeneous Photo-Fenton Process Mediated by Prussian Blue Colloids. *J. Hazard. Mater.* **2010**, *182*, 665–671. [[CrossRef](#)]
51. Singh, S.; Pandey, P.C. Synthesis and Application of Functional Prussian Blue Nanoparticles for Toxic Dye Degradation. *J. Environ. Chem. Eng.* **2020**, *8*, 103753. [[CrossRef](#)]
52. Ai, S.; Guo, X.; Zhao, L.; Yang, D.; Ding, H. Zeolitic Imidazolate Framework-Supported Prussian Blue Analogues as an Efficient Fenton-like Catalyst for Activation of Peroxymonosulfate. *Colloids Surf. A Physicochem. Eng. Asp.* **2019**, *581*, 123796. [[CrossRef](#)]
53. Zeng, H.; Deng, L.; Shi, Z.; Luo, J.; Crittenden, J. Heterogeneous Degradation of Carbamazepine by Prussian Blue Analogues in the Interlayers of Layered Double Hydroxides: Performance, Mechanism and Toxicity Evaluation. *J. Mater. Chem. A* **2019**, *7*, 342–352. [[CrossRef](#)]
54. Pi, Y.; Ma, L.; Zhao, P.; Cao, Y.; Gao, H.; Wang, C.; Li, Q.; Dong, S.; Sun, J. Facile Green Synthetic Graphene-Based Co-Fe Prussian Blue Analogues as an Activator of Peroxymonosulfate for the Degradation of Levofloxacin Hydrochloride. *J. Colloid Interface Sci.* **2018**, *526*, 18–27. [[CrossRef](#)] [[PubMed](#)]
55. Anipsitakis, G.P.; Dionysiou, D.D. Degradation of Organic Contaminants in Water with Sulfate Radicals Generated by the Conjunction of Peroxymonosulfate with Cobalt. *Environ. Sci. Technol.* **2003**, *37*, 4790–4797. [[CrossRef](#)] [[PubMed](#)]
56. Xiao, R.; Zhang, Y.; Wang, S.; Zhu, H.; Song, H.; Chen, G.; Lin, H.; Zhang, J.; Xiong, J. Prussian Blue Modified  $CeO_2$  as a Heterogeneous Photo-Fenton-like Catalyst for Degradation of Norfloxacin in Water. *Environ. Sci. Pollut. Res.* **2021**, *28*, 69301–69313. [[CrossRef](#)]
57. Jin, X.; Huang, Y.; He, S.; Chen, G.; Liu, X.; He, C.; Du, C.; Chen, Q. Preparation of Co-Fe Based Prussian Blue Analogs Loaded Nickel Foams for Fenton-like Degradation of Tetracycline. *Appl. Catal. A Gen.* **2023**, *650*, 118985. [[CrossRef](#)]
58. Khasevani, S.G.; Nikjoo, D.; Ojwang, D.O.; Nodari, L.; Sarmad, S.; Mikkola, J.-P.; Rigoni, F.; Concina, I. The Beauty of Being Complex: Prussian Blue Analogues as Selective Catalysts and Photocatalysts in the Degradation of Ciprofloxacin. *J. Catal.* **2022**, *410*, 307–319. [[CrossRef](#)]
59. Gögen, Y.; Koçak, Ç.C.; Karabiberoglu, Ş.; Polatdemir, E.; Aslaner, H.; Zorlu, R.; Çağlar, B.; Çirak, Ç.; Özdokur, K.V. Prussian Blue Modified Magnetite Decorated MW-CNT Nanocomposite: Synthesis, Characterization and Potential Use as Photo-Fenton Catalysts for Phenol Degradation. *Chem. Pap.* **2023**, *78*, 1863–1874. [[CrossRef](#)]
60. Srinivas, P.; Rajanna, K.C.; Krishnaiah, G.; Kumar, M.S.; Reddy, J.N. Prussian Blue as an Efficient Catalyst for Rate Accelerations in the Transesterification of  $\beta$ -Ketoesters. *Synth. React. Inorg. Met. Nano-Metal Chem.* **2014**, *44*, 1212–1220. [[CrossRef](#)]
61. Wang, Q.; He, S.; Wang, N.; Zhao, J.; Fang, J.; Shen, W. Synthesis of CoFe Prussian Blue Analogue/Carbon Nanotube Composite Material and Its Application in the Catalytic Epoxidation of Styrene. *New J. Chem.* **2016**, *40*, 3244–3251. [[CrossRef](#)]
62. Liang, Y.; Yi, C.; Tricard, S.; Fang, J.; Zhao, J.; Shen, W. Prussian Blue Analogues as Heterogeneous Catalysts for Epoxidation of Styrene. *RSC Adv.* **2015**, *5*, 17993–17999. [[CrossRef](#)]

63. Wang, Z.; Shi, G.; Xia, J.; Xia, Y.; Zhang, F.; Xia, L.; Song, D.; Liu, J.; Li, Y.; Xia, L.; et al. Facile Preparation of a Pt/Prussian Blue/Graphene Composite and Its Application as an Enhanced Catalyst for Methanol Oxidation. *Electrochim. Acta* **2014**, *121*, 245–252. [[CrossRef](#)]
64. Zhang, K.; Xiao, C.; Li, Y.; Li, C. Boosting Nucleophilic Attack to Realize High Current Density Biomass Valorization on a Tunable Prussian Blue Analogue. *Nanoscale* **2023**, *15*, 15649–15655. [[CrossRef](#)] [[PubMed](#)]
65. Pasnoori, S.; Kamatala, C.R.; Mukka, S.K.; Kancharla, R.R. Prussian Blue as an Eco-Friendly Catalyst for Selective Nitration of Organic Compounds under Conventional and Nonconventional Conditions. *Synth. React. Inorg. Met. Nano Metal Chem.* **2014**, *44*, 364–370. [[CrossRef](#)]
66. Marquez, C.; Cirujano, F.G.; Van Goethem, C.; Vankelecom, I.; De Vos, D.; De Baerdemaeker, T. Tunable Prussian Blue Analogues for the Selective Synthesis of Propargylamines through A3 Coupling. *Catal. Sci. Technol.* **2018**, *8*, 2061–2065. [[CrossRef](#)]
67. Zheng, M.W.; Lai, H.K.; Lin, K.Y.A. Valorization of Vanillyl Alcohol by Pigments: Prussian Blue Analogue as a Highly-Effective Heterogeneous Catalyst for Aerobic Oxidation of Vanillyl Alcohol to Vanillin. *Waste Biomass Valorizat.* **2019**, *10*, 2933–2942. [[CrossRef](#)]

**Disclaimer/Publisher's Note:** The statements, opinions and data contained in all publications are solely those of the individual author(s) and contributor(s) and not of MDPI and/or the editor(s). MDPI and/or the editor(s) disclaim responsibility for any injury to people or property resulting from any ideas, methods, instructions or products referred to in the content.